Intramolecular rearrangements guided by adaptive coordination-driven reactions toward highly luminescent polynuclear Cu(i) assemblies

M. El Sayed Moussa, A.M. Khalil, S. Evariste, H.-L. Wong, V. Delmas, Boris Le Guennic, Guillaume Calvez, K. Costuas, V.W.-W. Yam, Christophe Lescop

Intramolecular rearrangements guided by adaptive coordination-driven reactions toward highly luminescent polynuclear Cu(I) assemblies

Mehdi El Sayed Moussa,[a] Ali Moustafa Khalil,[a] Sloane Evariste,[a] Hok-Lai Wong,[b] Vincent Delmas,[a] Boris Le Guennic,[a] Guillaume Calvez,*[a] Karine Costuas,*[a] Vivian Wing-Wah Yam,*[b] Christophe Lescop*[a]

Adaptive coordination-driven supramolecular chemistry based on conformationally flexible pre-organized luminescent Cu(I) precursors paves the way to the ready formation of intricate supramolecular scaffold possessing intrinsic luminescence properties. A formal ring extension of a tetrametallic Cu(I) metallacycle bearing Thermally Activated Delayed Fluorescence (TADF) properties can thus be carried out, affording a new hexametallic Cu(I) metallacycle **1** bearing modulated solid-state TADF properties. Attempts to adapt this ring extension process to the formation of targeted heterometallic Au_2Cu_4 and Pt_2Cu_8 assemblies led to the unexpected and ready formation of the Au_2Cu_{10} and Pt_4Cu_{11} derivatives **2** and **3**, respectively. These outcomes strengthen the scope and perspectives of adaptive coordination-driven supramolecular chemistry compared to those of conventional coordination-driven supramolecular chemistry. Indeed, it guides concerted intramolecular fragmentation and redistribution of the particular building blocks used, affording selectively supramolecular scaffolds of higher nuclearity and complexity. The study of the solid-state photophysical properties of the assemblies **2** and **3** highlights enhanced and original behaviors, in which the heavy metal spin-orbit coupling values significantly influence the relaxation processes centered on the Cu(I) metal centers.

Introduction

An intense research activity is currently focused on the synthesis and study of advanced supramolecular architectures bearing increased structural complexity and new functionalities.[1] To this end, coordination-driven supramolecular (CDS) chemistry[2] offers a largely used synthetic tool to build such assemblies. This bottom-up approach uses robust, reversible and directional metal-to-ligand coordinative bonds to selectively build intricate metallo-supramolecular architectures.

Importantly, among the manifold functionalities that have been embedded into CDS assemblies, luminescence has been seldom investigated[3,4] and the potential of light-emitting CDS derivatives remains mostly unexplored. In most of the studies conducted so far in this field, the emission behaviors observed in CDS assemblies are either due to the intrinsic fluorescence properties of the π-conjugated multitopic linkers[3] or to those of the heavy metals (Pt(II), Re(I), Ir(III), Au(I), Pd(II) or Ru(II) ions)[4] based phosphorescent building blocks used. Cu(I) coordination complexes currently witness a great attention because of the fascinating photophysical properties they can exhibit.[5] These emission behaviors are characterized by the large diversity of the radiative relaxation processes involved but a rising attention is paid to derivatives exhibiting Thermally Activated Delayed Fluorescence (TADF).[5,6] In such complexes, thermally activated population of the lowest energy excited singlet state (S_1) from the lowest energy triplet excited state (T_1) occurs, inducing efficient radiative relaxation to the ground state and room temperature solid-state luminescence properties.

Yet, to date, the attractiveness of Cu(I) TADF luminescent precursors acting as pre-organized building blocks to conduct general CDS syntheses toward emissive coordination-driven supramolecular assemblies remains to be evaluated. Indeed, it is commonly accepted that the Cu(I) ion presents a labile and fluxional coordination sphere that is *a priori* not sufficiently directional to allow one to conduct such selective CDS synthetic processes. In this context, we have recently shown that this limitation can be overcome using pre-assembled Cu(I) bimetallic molecular clips bearing short intermetallic distances, allowing the general and versatile CDS preparation of a large family of stacked supramolecular assemblies.[2f] We have

[a] *Univ Rennes, INSA Rennes, CNRS, ISCR (Institut des Sciences Chimiques de Rennes) – UMR 6226, F-35000 Rennes, France. E-mails : guillaume.calvez@insa-rennes.fr; karine.costuas@univ-rennes1.fr; christophe.lescop@insa-rennes.fr*

[b] *Institute of Molecular Functional Materials [Areas of Excellence Scheme, University Grants Committee (Hong Kong)] and Department of Chemistry, The University of Hong Kong, Pokfulam Road, Hong Kong, P.R. China. E-mail : vwyam@hku.hk*

† Footnotes relating to the title and/or authors should appear here.

Electronic Supplementary Information (ESI) available: experimental, theoretical, analytical and crystallographic details. For ESI and crystallographic data in CIF or other electronic format see DOI: 10.1039/x0xx00000x

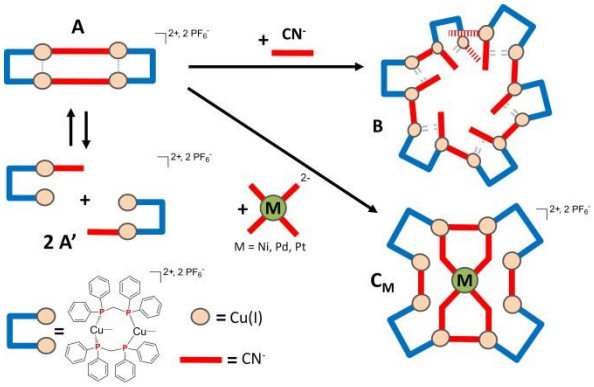

Scheme 1 Synthetic scheme of the adaptive CDS preparation of the one-dimensional helicoidal coordination polymer **B** and the discrete Cu_8M_1 supramolecular assemblies $\mathbf{C_M}$ from precursor **A**.[7b]

recently extended this CDS approach to the use of a pre-assembled TADF Cu(I) precursor, the tetrametallic metallacycle **A**,[7a] affording the first adaptive CDS preparations of polymetallic Cu(I) supramolecular assemblies (Scheme 1) bearing various architectures and intrinsic solid-state luminescent properties.[7b]

Herein, we first report that this adaptive CDS approach can be extended to the reaction of **A** with CuCN, acting as an alternative cyano-based precursor, to allow isolation of a new highly luminescent hexametallic Cu(I) assembly **1** via a formal inorganic ring extension process. More importantly, considering such outcome, we have been prompted to conduct CDS reaction between the pre-assembled bimetallic precursor $[Cu_2(\mu_2\text{-dppm}_2)(CH_3CN)_4](PF_6)_2$ with $K[AuCN_2]$ and $K_2[PtCN_4]$ building blocks. Unprecedented highly luminescent multimetallic $Cu_{10}Au_2$ derivative **2** and $Cu_{11}Pt_4$ derivative **3** were obtained respectively via a one-step reaction self-assembly processes. The selective formation of these intricate supramolecular assemblies can be rationalized as resulting from concerted rearrangement of the building blocks guided by adaptive CDS processes. These results suggest that adaptive CDS syntheses can direct unprecedented single-step syntheses toward polymetallic species having unique structural and luminescence properties.

Results and discussion

Adaptive CDS preparation of the Cu_6 metallacycle 1

In a first step, in order to study whether the adaptive CDS processes conducted from **A** (Scheme 1)[7b] could be extended to other cyano-based building blocks, **A** was reacted with CuCN in a 1:2 ratio (Fig. 1). As the colorless CH_2Cl_2 solution of the metallacycle **A** was mixed under air at room temperature (RT) with a methanol solution of CuCN, neither color changes nor precipitates were observed.[8] The $^{31}P\{^1H\}$ NMR spectra of the mother solution recorded in CD_2Cl_2 reveals one broad multiplet centered at $\delta = -11.0$ ppm showing no significant shift compared to the signals observed for **A** (two broad singlets at $\delta = -8.5$ ppm and -10.5 ppm).[7a] These solution data suggest that the putative reaction of CuCN with **A** induces minimal molecular reorganization in the new species eventually formed, which would still be based on $[Cu_2(\mu_2\text{-dppm})_2]$ units. As pentane vapors were diffused into the mother solution for one week, a mixture of two kinds of colorless single crystals was obtained. These crystals are hardly distinguishable under visible light but it was possible to separate them manually under UV irradiation (λ_{ex} = 365 nm) since they display markedly different eye-perceived intense blue or green solid-state RT luminescence. X-ray diffraction studies[8] performed at low temperature on single crystals revealed that the solid-state blue luminophore is the precursor **A** while the solid-state green luminophore is a new hexametallic Cu(I) metallacycle **1** (Fig. 1). The derivative **1** could be collected pure after careful manual separation with a yield of ca. 20 %.[8] The asymmetric unit of the new derivative **1** contains one half of a dicationic $[Cu_6(CN)_4dppm_4]^{2+}$ discrete assembly, one hexafluorophosphate counter-anion and two disordered CH_2Cl_2 solvent molecules. In this Cu_6 metallacycle **1**, two peripheral $[Cu_2(\mu_2\text{-dppm})_2]^{2+}$ fragments are connected by two almost linear NC-Cu_{inner}-CN moieties[9] (C-Cu_{inner}-C = 177.48(15)°), leading to a planar 'Cu_6CN_4' diamond-shape metallacycle (maximum deviation from the mean plane, 0.05 Å, Fig. 1a). The metric parameters of the $[Cu_2(\mu_2\text{-dppm})_2]^{2+}$ units are very similar to those observed in the solid-state structure of **A** with, in particular comparable intermetallic distances (2.8806(8) Å in **1**; 2.8669(6) Å in **A**) relevant for cuprophilic interactions. Conversely, inner Cu(I) metal centers belonging to the NC-Cu_{inner}-CN connecting moieties are separated by ca. 3.78 Å which is too large for metallophilic interactions. Importantly, in the crystal packing, neighboring metallacycles are found to be closely interconnected with short contact interactions observed between the Cu_{inner} metal centers, the cyano fragments and the phenyl rings of the neighboring discrete assemblies (d ≤ 2.8 Å, Fig. 1b). Temperature-dependent X-ray diffraction studies were performed on the same single crystal of **1** at 25 K intervals from 100 K to 250 K. These measurements reveal a progressive and moderate shrinkage of the unit cell volume upon cooling, from 6007(2) $Å^3$ (250 K) to 5791.8(4) $Å^3$ (100 K) (ca. 3.7% of volume contraction). This volume contraction mostly affects the relative molecular arrangement between the PF_6^- counter-anions, the included solvent molecules and the peripheral dppm phenyl rings. Along these measurements, a very slight alteration of the metric parameters around the metal centres in this Cu_6 metallacycle is observed: the $[Cu_2(\mu_2\text{-dppm})_2]^{2+}$ intermetallic distances presented a 1.2% of length contraction (from 2.9083(11) Å at 250 K to 2.8806(8) Å at 100 K) while the inner intermetallic distance bears a 0.7 % of length contraction (from 3.797(12) Å at 250 K to 3.769(9) Å at 100 K). Notably, similar to what was observed in the temperature dependence of solid-state X ray structure of the precursor **A**,[7a] the whole dimension and shape of the metallacyle are kept unchanged (Table S4). Therefore, the

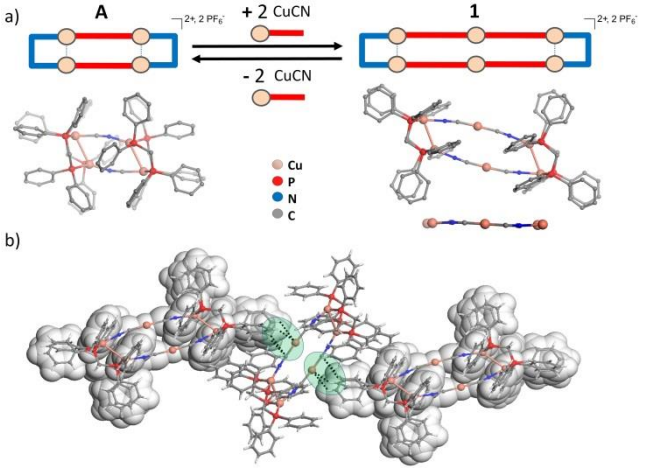

Fig. 1. a) Syntheses of the derivative **1** and comparative views of the X-ray crystal structures of **A**[7a] (top view) and **1** (top view and lateral simplified view; counteranions, H atoms and solvent molecules have been omitted for clarity; location of the C and N atoms of the cyano ligands has been chosen arbitrarily). b) View of the short contact intermolecular interactions (shown with dotted lines in the green ellipses) observed between neighboring imbricated metallacycles in the crystal structure.

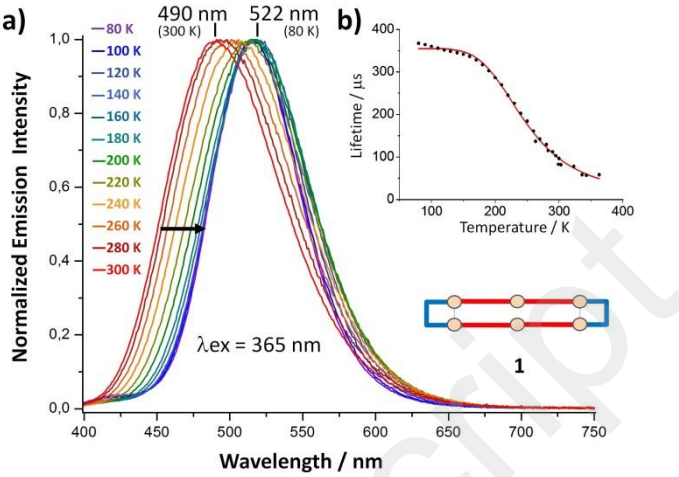

Fig. 2. a) Normalized solid-state emission spectra of **1** at temperatures between 80 K and 300 K upon excitation at 365 nm, the black arrow shows the direction of the thermochromic shift of the solid-state emission spectra observed upon cooling; b) plot of emission decay lifetime against temperature (80 K to 363 K); The red line represents the fit according to the TADF Boltzmann-type Equation S1.

thermochromic luminescence (*vide infra*) observed for the derivative **1** cannot be interpreted based on a temperature-dependence of its ground state molecular arrangement.

Crystalline samples of **1** display at 300 K an eye-perceived intense green luminescence upon excitation at 365 nm (Fig. 2). This corresponds to a broad and featureless emission band with an emission maximum λ_{em} at 490 nm, a monoexponential emissive lifetime τ of 80 µs and an emission quantum yield (EQY) that reaches 80 %. Upon cooling, the emission spectrum of derivative **1** presents a gradual red-shift of the emission band observed, affording an intense solid-state eye-perceived yellowish luminescence at low temperature (Fig. 2: λ_{em} = 522 nm at 80 K and τ = 365 µs). Upon heating up from RT to 363 K, very moderate thermal variations of both the emission spectrum (Fig. S17) and the lifetime are observed, reaching a plateau region at ca. 330 K with λ_{em} = 487 nm ($\Delta\lambda_{em\ 80K/363K}$ = 0.132 eV / 1065 cm^{-1}) and τ = 57 µs. Such emission behavior is typical of Cu(I) derivatives showing thermally activated delayed fluorescence (TADF).[5a,6] By fitting the thermal evolution of τ to the Boltzmann-type equation S1 in SI, the values of $\Delta E(S_1\text{-}T_1)$ = 1023 cm^{-1}, $\tau(S_1)$ = 325 ns and $\tau(T_1)$ = 352 µs could be obtained (Fig. 3a). Despite this set of values being significantly different from those obtained for the tetrametallic precursor **A** ($\Delta E(S_1\text{-}T_1)$ = 1560 cm^{-1}, $\tau(S_1)$ = 10 ns and $\tau(T_1)$ = 185 µs),[7a] both can be accounted for TADF processes.

In order to get more insights in the energetics and emission properties of **1**, a DFT / TD-DFT computational study was performed (see SI for computational details). The high computational cost needed for full excited states investigations prevents us to use larger atomic basis sets. First, a conformational computational study was performed, indicating that the arrangement presented in Fig. 1, bearing Cu-N≡C-Cu_{inner}-C≡N-Cu fragments, is the most probable isomer (see SI and Scheme S1) that will be used for the computational investigation.The main results obtained for the ground state **1**-S_0 and its lowest singlet and triplet relaxed excited states (**1**-S_x and **1**-T_x, x = 1 - 3) are summarized in Fig. 3b and Tables S5 and S6. The DFT optimized geometry of S_0 compares well with the experimental X-ray structure with $[Cu_2(\mu_2\text{-dppm})_2]^{2+}$ intermetallic distances of 2.854 Å (exp.: 2.8806(8) Å) and $Cu_{inner}\cdots Cu_{inner}$ contact of 3.84 Å (exp.: 3.78 Å). TD-DFT calculations reveal that the first singlet-singlet electronic vertical excitation consists of an electronic density transfer mainly from the close surrounding of the Cu atoms of the $[Cu_2(\mu_2\text{-dppm})_2]^{2+}$ moieties to the interstitial Cu-Cu region, and to a lesser extent, to the CN bridges and phosphorus atoms of the dppm ligands (see Fig. S26). This mainly induces a strengthening of the Cu-Cu interaction. Interestingly, geometry relaxation following this excitation leads to a symmetry lowering in which only one of the two Cu-Cu distances in $[Cu_2(\mu_2\text{-dppm})_2]$ is shortened (2.592 Å) whereas the other one is mildly lengthened (2.903 Å). These changes are associated with a translation between the Cu-NC-Cu_{inner}-CN-Cu segments which lead to a more rectangular shape of the metallacycle (Fig. 3). The central $Cu_{inner}\cdots Cu_{inner}$ separation is concomitantly enlarged (3.975 Å). Similar changes are also calculated for the close energy-lying excited states **1**-S_2, **1**-S_3 and for the first triplet states **1**-T_1. Interestingly for the latter, additional expansion of the metallacycle with a $Cu_{inner}\cdots Cu_{inner}$ separation of 4.181 Å is observed. Contrary to the translational motion that leads to a more rectangular metallacycle that is observed for the first singlet excited states, this expansion is expected to be hampered by crystal packing. Indeed, as shown in Fig. 1b, short intermolecular contacts are observed between the Cu_{inner}

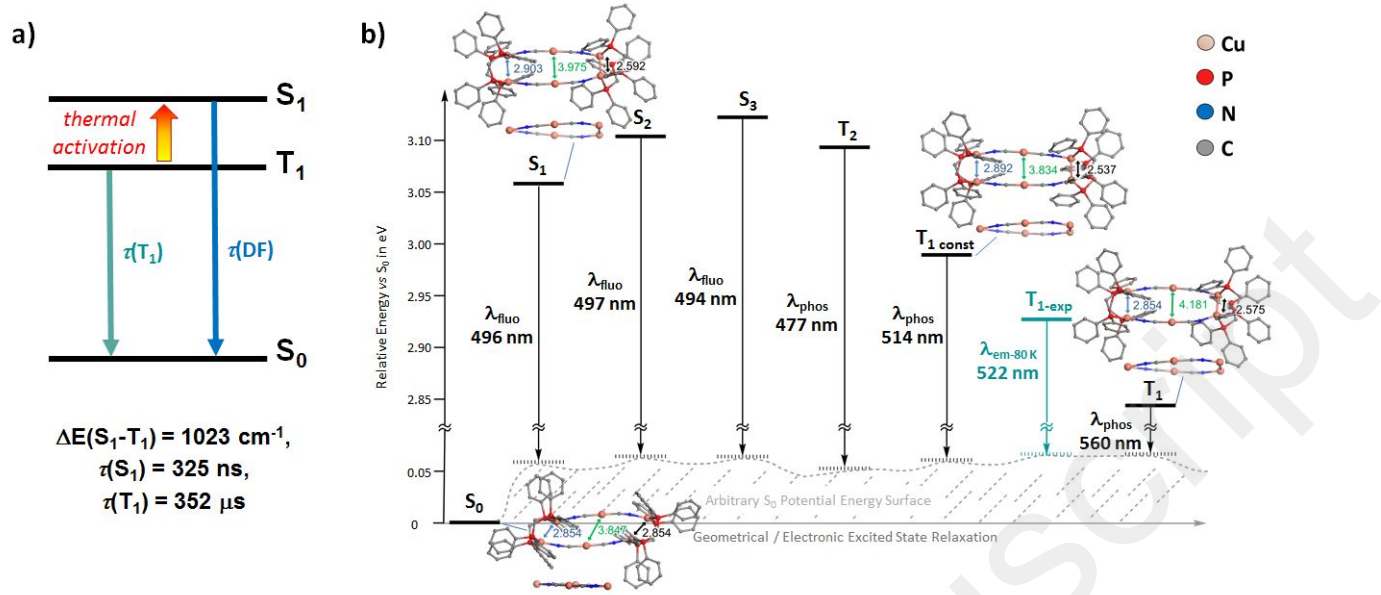

Fig. 3. a) Scheme of the TADF process and photophysical values experimentally obtained. b) Relative energy diagram of the first optimized excited states relatively to S_0 in eV; associated emission wavelengths in nm; see Table S5 for a complete summary of the emission energies. Top view and lateral views of the optimized geometries of **1**-S_0, **1**-T_1, **1**-T_{1const} and **1**-S_1 (H atoms omitted); intermetallic Cu-Cu distances (in Å). Experimental T_1 level ($T_{1\text{-}exp}$) and associated experimental values in green for the sake of comparison.

and cyano fragments with the phenyl rings of the neighboring metallacycle (d ≤ 2.8 Å). To take into account these solid-state environment hindrances, a constrained geometry optimization was performed for the first triplet state restraining the $Cu_{inner}\cdots Cu_{inner}$ elongation to not exceed the one found in **1**-S_1. This constrained optimization gave rise to the system **1**-$T_{1\text{-}const}$ (see Fig. 3 and Tables S5 and S6). The emission energies calculated from these relaxed excited state structures nicely explain the experimental optical measurements. Indeed, the calculated wavelength of fluorescence (from **1**-S_1) (496 nm) agrees well with the emission maximum measured at 300 K (490 nm, Fig. 2a). At low temperature (80 K), the experimental wavelength is at 522 nm and the emission lifetime is indicative of a phosphorescence process (Fig. 2). The calculated emission wavelength of **1**-$T_{1\text{-}const}$ is at 514 nm. The discrepancies between experimental and calculated emission energies is of ca. 0.04 eV which is in line with the level of theory used. The calculated total energy differences between **1**-S_1 and the first excited triplet states **1**-T_1 and **1**-$T_{1\text{-}const}$ are of 533 cm^{-1} and 1703 cm^{-1} respectively. The intermediate value of 1023 cm^{-1} extracted from the fit of the experimental lifetime dependence toward temperature suggests that indeed **1**-$T_{1\text{-}exp}$ adopts very likely a conformation in the solid-state in which the metallacycle expands moderately as a result of intermolecular steric hindrance constraints. All in all, these computational results support a TADF process for **1** (see Fig. 3a). The moderate values of calculated spin-orbit coupling energies given in Table S7 are slightly larger than those determined for **A**[7a] and are in agreement with a competition between Inter-System Crossing (ISC)/Reverse Inter-System Crossing (RISC) and thermal population of S_1 from T_1. Moreover, the strong similarities between the geometries of S_1 and T_1 give further support to the TADF process.

As previously suggested for the formation of derivatives **B** and $\mathbf{C_M}$ (Scheme 1),[7b] the synthesis of the hexametallic species **1** can be explained by considering the reversible dissociation of the tetrametallic **A** derivative in two coordinatively unsaturated reactive Cu(I) dimers **A'** in the adaptive CDS process. In the present case, CuCN moieties can be coordinated to **A'** and the resulting fragments subsequently re-associate resulting *in-fine* in a formal inorganic ring extension. Importantly, despite several attempts to optimize the reaction conditions, the selective preparation of the derivative **1** was not successful, converse to what was observed in the preparation of **B** and $\mathbf{C_M}$.

Instead, similar mixtures of crystals of **A** and **1** were always collected. Considering the similarities observed in the crystal structures of **A** and **1** (Fig. 1), it is very likely that the thermodynamic stabilization of **1** toward **A** is not sufficient to promote a displacement of the equilibria toward a quantitative formation of **1**.[10] Interestingly, a similar situation was reported by Koshevoy *et al.* in the preparation of zig-zag one-dimensional polymers bearing either LCu(I)-CN-Cu(I)L or LCu(I)-CN-Cu(I)-CN-Cu(I)L linear fragments (L = 1,2-bis(diphenyl phosphino)benzene).[11] Importantly, the formation of **1** confirms the reversible dissociative mechanism of **A** suggested,[7b] which can explain the adaptive CDS syntheses conducted from this luminescent building block.

Syntheses of the $Cu_{10}Au_2$ derivative 2 and of the $Cu_{11}Pt_4$ derivative 3

Considering that the inner intermetallic distance observed in assembly **1** (ca. 3.78 Å) lies in the upper limit of those usually accepted for stabilizing Au(I)-Au(I) interactions,[12] we anticipated that a replacement of the inner linear Cu(I) metal centers by Au(I) ions could promote a displacement of solution equilibria toward the selective synthesis of a new compact hexametallic assembly. A 'Cu_4Au_2' complex **2'** would result (Scheme 2) associating within one compound the original photophysical properties of TADF Cu(I) centers and those of Au(I) metal ions involved in aurophillic interactions. Inspired by previous CDS syntheses of related compact 'Cu_4Au_2' species resulting from the reaction of a rigid 'U-shape' Cu(I) bimetallic clips with $K[Au(CN)_2]$,[2f,13] we choose to react the pre-assembled bimetallic Cu(I) complex $[Cu_2(dppm)_2(CH_3CN)_4](PF_6)_2$ (**D**) with $K[Au(CN)_2]$ (Scheme 2). In addition, precursor **D** was also reacted with $K_2[Pt(CN)_4]$ to explore whether stabilizing lateral Pt(II)-Pt(II) metal-metal interactions[14] could also drive the preparation of new 'Cu_8Pt_2' compact three-dimensional luminescent assemblies **3'** (Scheme 2) bearing both TADF Cu(I) metal centers and Pt(II)-Pt(II) metal-metal interactions.[14]

Colorless CH_2Cl_2 solutions of in-situ prepared derivative **D** were thus mixed under air at RT in 1:1 ratio with, respectively, 10:1 water/acetonitrile solution of $K[Au(CN)_2]$ and methanol solution of $K_2[Pt(CN)_4]$. $^{31}P\{^1H\}$ NMR spectra of the resulting clear colorless solutions showed, respectively, four broad singlets centered at ca. −14.5, +30.4, +34.4 and +37.0 ppm and a broad multiplet between –21.0 and −12.0 ppm accompanied by a doublet centered at +3.0 ppm with satellites corresponding to $^1J_{P,Pt}$ = 2590 Hz. These spectroscopic data suggest that reactions occurred in both cases since the typical signal of unreacted precursor **D** (–8.9 ppm)[15] was not observed. Yet, the downfield shifted signals observed in each spectrum are very intriguing considering the targeted supramolecular assemblies. Indeed, it is not expected to observe such sets of signals if all the $[Cu_2(\mu_2\text{-dppm})_2]^{2+}$ fragments are preserved in these reactions. Pentane vapor diffusions in the organic mother solutions allowed the isolation of derivatives **2** and **3** as colorless needles single crystals, in 83 % and 87 % yields respectively.[8] Solid-state infrared spectrum shows for both compounds the presence of different cyano groups coordinated on the metal centers (ν(C≡N), **2**: 2124, 2149 cm^{-1}; **3**: 2121, 2137 cm^{-1}). In agreement with the $^{31}P\{^1H\}$ NMR spectra, these data suggest that derivatives **2** and **3** have gross molecular structures that are significantly different and less symmetrical than those of the targeted Cu_4Au_2 (**2'**) and Cu_8Pt_2 (**3'**) compounds (Scheme 2). The molecular structures of the derivatives **2** and **3** were established by X-ray diffraction studies revealing the unprecedented and unexpected formation of '$Cu_{10}Au_2$' (**2**) and '$Cu_{11}Pt_4$' (**3**) discrete supramolecular assemblies. The asymmetric unit of **2** contains one '$Cu_{10}Au_2$' dicationic discrete assembly, two PF_6^- anions and twelve CH_2Cl_2 solvent molecules.

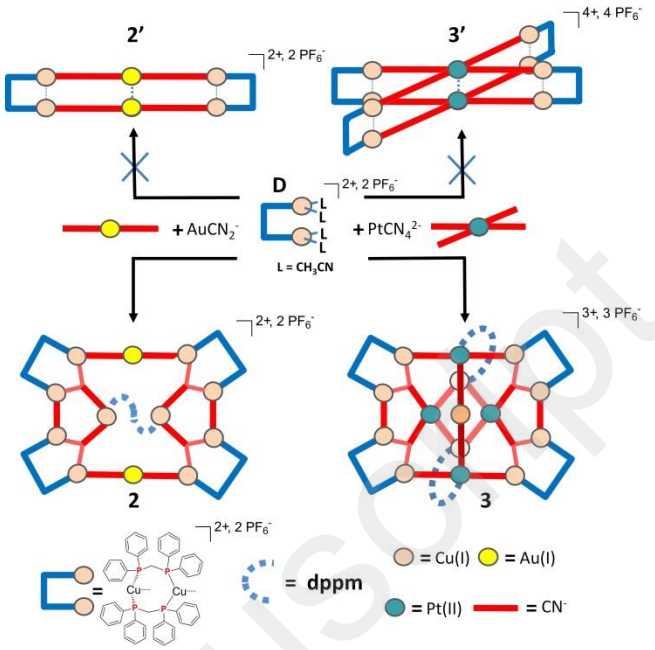

Scheme 2 Molecular schematic backbones of the initially targeted assemblies **2'** and **3'** and syntheses of the derivatives **2** and **3**.

In the polymetallic derivative **2** (Fig. 4), four peripheral $[Cu_2(\mu_2\text{-dppm})_2]^{2+}$ moieties lie on the corners of a 'Cu_8Au_2' rectangular-shaped metallacyclic unit. These $[Cu_2(\mu_2\text{-dppm})_2]^{2+}$ moieties are connected two by two by one CN^- linker[9] acting in a linear μ_2-coordination mode. The resulting two '$[Cu_2(\mu_2\text{-dppm})_2\text{-CN-}Cu_2(\mu_2\text{-dppm})_2]$' fragments are bridged by two almost linear NC-Au-CN ditopic fragments (C-Au-C, ca 175°), forming therefore the 'Cu_8Au_2' metallacyclic unit. In addition, each of the four $[Cu_2(\mu_2\text{-dppm})_2]^{2+}$ moieties is also coordinated to a μ_3-cyano ligand that connects the bimetallic units of these four peripheral $[Cu_2(\mu_2\text{-dppm})_2]^{2+}$ moieties to a central $[Cu_2(dppm)]$ fragment. A '$Cu_{10}Au_2(CN)_{10}$' inorganic core (Fig. 4) is thus formed, having an almost planar discoidal shape (maximum deviation from the mean plane, 0.8 Å). The intermetallic peripheral Cu(I) distances range from ca. 2.9 Å to 3.0 Å which is the upper limit of Cu(I)-Cu(I) distances relevant for cuprophilic interactions. Conversely, the intermetallic central Cu-Cu and the Au-Au distances, respectively above, 4.5 Å and 11.1 Å, are too large for metallophilic interactions. The asymmetric unit of **3** contains one half of a '$Cu_{11}Pt_4$' tricationic assembly, 1.5 PF_6^- anions and twelve CH_2Cl_2 solvent molecules. Similarly to what is observed in the derivative **2**, a 'Cu_8Pt_2' rectangular-shaped metallacyclic sub-unit (Fig. 5a) can be firstly defined in which four $[Cu_2(\mu_2\text{-dppm})_2]^{2+}$ moieties are connected either by CN^- linkers, or linear NC-Pt-CN fragments.[9] These Pt(II) metal ions' coordination sphere is square planar, being completed by a connection to an almost linear central NC-Cu-CN fragment (C-Cu-C, 177.1(3)°) that bridges these two Pt(II) metal centers, and by a phosphorus atom of a dppm ligand acting as a 1κ*P*:2κ*P* chelate on an unexpected Pt(II)-Cu(I) heterometallic dimer. Finally, the Cu(I)

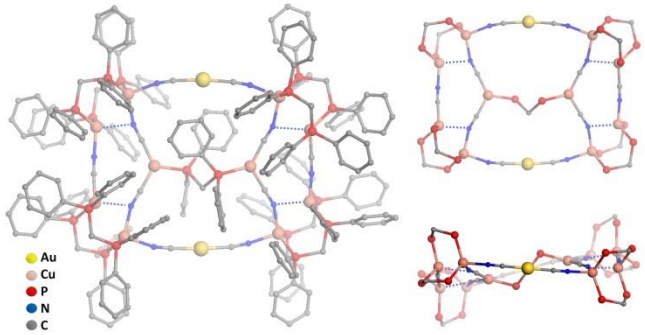

Fig. 4. General views and simplified 'top' and side views of molecular X-ray structure of derivative **2** (counter-anions, H atoms, solvent molecules and phenyl rings of the dppm ligands in the simplified views have been omitted for clarity; location of the C and N atoms of the cyano ligands has been chosen arbitrarily except for the $Au(CN)_2$ fragments).

centers of the peripheral $[Cu_2(\mu_2\text{-dppm})_2]^{2+}$ moieties have their coordination sphere completed by μ_3-cyano ligands belonging to two distorted square planar $Pt(CN)_4$ units. The two other cyano moities of these $Pt(CN)_4$ fragments act as μ_2-linkers to connect these Pt(II) centers to the distorted trigonal planar Cu(I) metal atom of the Pt(II)-Cu(I) heterobimetallic units. As a result, a '$Cu_{11}Pt_4dppm_{10}(CN)_{16}$' inorganic core (Fig. 5) having a unique "basket with handle" shape is formed. The peripheral Cu(I)-Cu(I) and the intermetallic Pt(II)-Cu(I) distances are, respectively, from ca. 3.0 Å to 3.2 Å and ca. 2.95 Å. No intermetallic Pt(II)-Pt(II) short distances are observed (d(Pt-Pt) > 5.6 Å). Considering the solid-state crystal packing, while no specific intermolecular interactions are observed in the case of compound **2**, a remarkable extended non-covalent network is built upon the crystallisation of **3**. Indeed, these large polymetallic species (ca 28 Å × 28 Å × 17.2 Å) first self-aggregates through strong and cumulative π-π and π-CH interactions in cyclic trimers (Fig. 5b). Then these trimeric units would arrange in the bulk crystalline solid due to additional π-π, π-CH and anion-π interactions leading to a three-dimensional network in which large hexagonal channels (Fig. 5b, cross-section ca. 28 Å × 28 Å) filled by solvent molecules and anions are observed. Solid-state samples of **2** and **3** display intense luminescence properties at room temperature. Crystalline samples of the '$Cu_{10}Au_2$' derivative **2** and the '$Cu_{11}Pt_4$' derivative **3** display at 300 K, respectively (Fig. 6), an eye-perceived yellowish luminescence (**2**: λ_{max} = 520 nm with λ_{ex} = 330 nm) and cyan luminescence (**3**: λ_{max} = 492 nm with λ_{ex} = 350 nm). These emission spectra are characterized by a broad and featureless band (Fig.s 6 and 7). For derivative **2**, a bi-exponential decay time of ca. τ_1 = 6 μs and τ_2 = 17 μs is measured together with an EQY of 70%. For compound **3**, the emission decay is mono-exponential with τ = 11 µs and an EQY of 63 %. Upon cooling from 300 K to 80 K under excitation at 330 nm, an hypsochromic shift of the emission spectra of **2** is observed (Fig. 6a), leading to a broad band with an emission maximum of 503 nm at 80 K ($\Delta\lambda_{em\ 80K/300K}$ = 0.08 eV / 651 cm^{-1}) associated with an intense solid-state visually-perceived turquoise luminescence. Concomitantly, the emission decay remains bi-exponential and increases continually, reaching 12 μs for τ_1 and 58 μs for τ_2 at 80 K (Fig. 6b). Concerning compound **3**, the emission spectra exhibit a different behavior. With excitation at 385 nm, a progressive red-shift associated with the intense solid-state green-yellow luminescence at low temperature is observed (Fig. 6b, λ_{em} = 505 nm at 80 K ($\Delta\lambda_{em\ 80K/300K}$ = 0.065 eV / 524 cm^{-1})). The emission decay remains mono-exponential and increases almost linearly reaching the value of τ = 25 µs at 80 K.

Taking into account the large size of the molecules and the large influence of the solid-state packing on the geometry of such self-assembled structures (as witnessed by the analysis of the photophysical properties of **1** (*vide infra*), it is not possible to conduct full DFT geometry optimization of the excited states to get deep insights into the electronic origins of these different photophysical properties. Nevertheless, it is possible to state that the temperature dependences of the photophysical properties in **2** are suggestive of the lack of a TADF mechanism. The shift to the blue of emission maxima upon temperature variation is indeed not consistent with such a photophysical process. In general, a narrowing of the emission band width with decreasing temperature is observed, in line with the lower accessibility of higher vibrational states at low temperature. The blue shift at low temperature is also in agreement with the rigidochromic effect resulting from the increased rigidity at low temperature, leading to a smaller excited state distortion. Notably, such emission behavior resembles the luminescence properties observed for the helical compound **B** (Scheme 1),[6b] for which the RT emission band was assigned to Cu(I) metal- perturbed dppm ligand-centered phosphorescence and the higher-energy emission band at low temperature to a metal-to-ligand charge transfer (MLCT) [dσ*(Cu)→ π*(CN)/ π*(dppm)] state with mixing of a copper-centered d-s/d-p excited states. Thermal variation of the bi-exponential decay times τ1 and τ2 also support the assumption of multiple emission processes but the values determined, in particular at RT are too short for purely phosphorescence processes. Very likely, despite no aurophilic interactions are observed in the solid-state structure of **2**, the Au(I) atoms would have an influence on the photophysical processes in derivative **2**. As previously observed in the case of the emission behavior of $\mathbf{C_{Pt}}$ (Scheme 1), a minor but significant electron density located on the Au(I) metal centers in the excited states would be sufficient to promote enhancement of the spin-orbit coupling components in the whole radiative processes, due to the contribution of the high spin-orbit coupling constant of the Au(I) ions. This would account for the relatively short emission decay times associated to radiative processes mostly centered on the Cu(I) ions. Regarding the photophysical properties of derivative **3**, while the bathochromic shift of its emission spectra upon temperature cooling resembles those typically described for Cu(I) TADF derivatives, the linear profile and the relatively short values associated with the temperature variation of the emission decay time do not support a pure TADF mechanism.

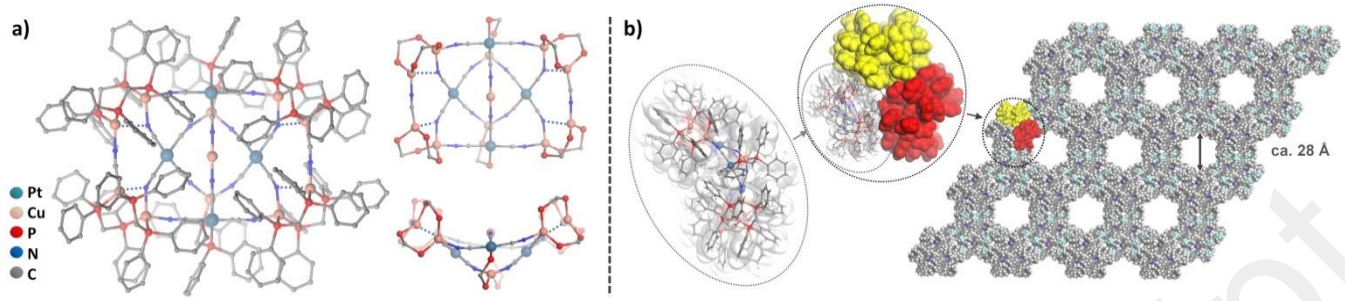

Fig. 5. a) General views and simplified 'top' and side views of molecular X-ray structures of derivative **3** (counteranions, H atoms, solvent molecules and phenyl rings of the dppm ligands in the simplified views have been omitted for clarity; location of the C and N atoms of the cyano ligands has been chosen arbitrarily except for the $Pt(CN)_x$ fragments, x = 3 or 4); b) Solid-state organization observed in the single crystals of the derivative **3**.

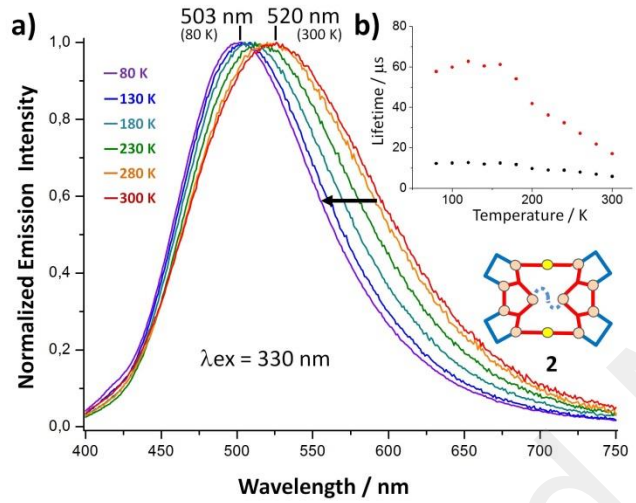

Fig. 6. a) Normalized solid-state emission spectra of **2** at temperatures between 80 K and 300 K upon excitation at 330 nm (the black arrow shows the direction of the thermochromic shift of the solid-state emission spectra observed upon cooling); b) plots of emission decay lifetimes against temperature (80 K to 300 K, red dots for the long component and black dots for the short component).

The profile and absence of plateaus in the thermal variation of the emission decay time forbid application of a meaningful TADF fit. Similarly to **2**, the complexity of the polymetallic supramolecular architecture observed in **3** suggests the possibility of a temperature dependent competition of several deactivation processes arising from multiple Cu(I) sites. A contribution of the Pt(II) ions via their high spin-orbit coupling constants is also likely to occur. As observed for the related 'Cu_8Pt_1' compound $\mathbf{C_{Pt}}$[7b] and for **2**, it would induce an enhancement of the non-radiative and radiative processes arising from singlet excited states in **3** resulting in a competition between ISC to give phosphorescence and RISC to give TADF. Importantly, the RT EQY of **3** (63 %) presents a remarkable enhancement compared to $\mathbf{C_{Pt}}$[7b] (18 %). The origin of such an increase is not straightforward to assign but is likely to be related with a higher extent of the interactions between the Cu(I) and Pt(II) metal centers (including the 'PtCu(μ_2-dppm)' heterodimer in **3**). All in all, these photophysical data highlight that the high structural complexity observed in **2** and **3** is accompanied with the observation of unusual and enhanced solid-state luminescence properties. The large discrepancy observed between the targeted supramolecular structures **2'** and **3'** (Scheme 2) and those of **2** and **3**, selectively and reproducibly obtained, raises the question of the self-assembly processes that are implemented in their formation. Along these syntheses, the $[Cu_2(\mu_2\text{-dppm})_2]^{2+}$ unit keeps its unique flexibility (modulation of the intermetallic distances and the coordination bite angle of the chelating dppm ligands) allowing one to conduct adaptive supramolecular syntheses as observed for the preparation of **B** and $\mathbf{C_M}$ (Scheme 1).

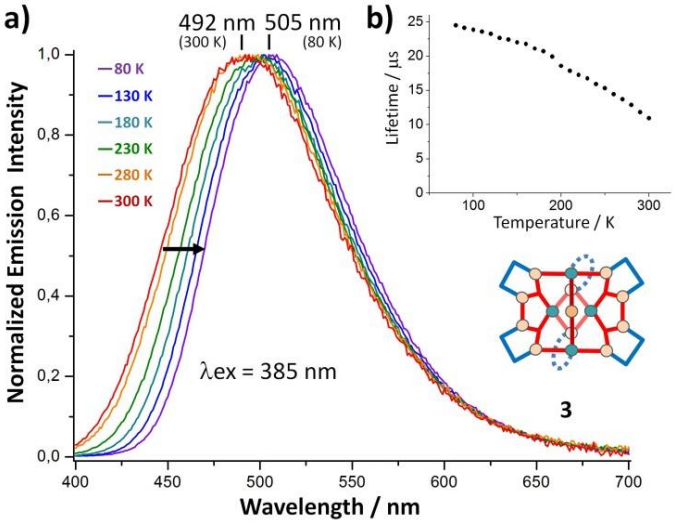

Fig. 7. a) Normalized solid-state emission spectra of **3** at temperatures between 77 K and 300 K upon excitation at 385 nm (the black arrow shows the direction of the thermochromic shift of the solid-state emission spectra observed upon cooling); b) plot of emission decay lifetime against temperature (80 K to 300 K).

Nevertheless, the scope of the self-assembly processes goes further, highlighting new aspects of adaptive CDS processes. While in conventional CDS,[3] initial building blocks' cores are preserved within the self-assembled structures, concerted dissociation of some cyano-based precursors and $[Cu_2(\mu_2\text{-dppm})_2]^{2+}$ fragments must occur at RT in both syntheses to yield the unprecedented supramolecular backbones of **2** and **3**. It is important to stress that the targeted assembly **2'** (Scheme 2) has a gross supramolecular architecture that is *a priori* accessible using CDS as proved by the previously reported preparation of 'Cu_4Au_2' compact metallacycles from the reaction of the rigid U-shape Cu(I) bimetallic molecular clip and $K[Au(CN)_2]$.[13] The conformational flexibility of the $[Cu_2(\mu_2\text{-dppm})_2]^{2+}$ unit offers thus a straightforward access to a higher nuclearity supramolecular scaffold. Moreover, the outcomes of the reaction of $K_2[Pt(CN)_4]$ with the pre-assembled precursor **A** (Scheme 1) or **D** (Scheme 2) are different affording, respectively, the 'Cu_8Pt_1' $\mathbf{C_{Pt}}$[7b] (Scheme 1) and the '$Cu_{11}Pt_4$' **3** derivatives. This allows excluding a full dissociation of the building blocks in the reaction conditions. Indeed, in such a situation, free cyano and dppm ligands[16] would be present in solution, leading to mixtures of self-assembled species (including **A**, $\mathbf{C_{Pt}}$ and **3**) in equilibrium. It is not expected that such equilibrium would afford selective preparation of the different derivatives $\mathbf{C_{Pt}}$ or **3**, depending on the reaction of the Cu(I) precursor (**A** or **D**) with $K_2[Pt(CN)_4]$.[17] Therefore it is very likely that concerted post-assembly intramolecular rearrangements would occur, and guided the adaptive CDS processes that can be conducted from the $[Cu_2(\mu_2\text{-dppm})_2]^{2+}$ unit to allow the selective preparation of the unprecedented scaffolds of **2** and **3**.

Conclusions

Adaptive CDS syntheses conducted from Cu(I) bimetallic precursors give a straightforward access to unprecedented polymetallic derivatives bearing attractive solid-state luminescence properties. Regarding the originality and the complexity of the supramolecular architectures obtained in these one-step syntheses from simple and commercially available building blocks, this new and alternative approach opens appealing and general perspectives in the preparation of innovative supramolecular scaffolds embedded with luminescence properties. Indeed, an overwhelming effort is currently devoted to the preparation of new multitopic organic ligands of various sizes, connectivities and functionalities to allow the preparation of advanced CDS architectures. A limiting counterpart that such trend in modern CDS implies is a pronounced tendency of ever-increasing complexity of the assembling ligand scaffolds. Eventually, this transposes to the overall molecular design of the targeted supramolecular architectures constraints and limitations of standard multistep synthetic chemistry that supramolecular self-assembling synthetic concepts somehow initially offered to overcome. The use of conformationally flexible Cu(I) polymetallic pre-assembled building blocks offers therefore an easy and alternative access for the preparation of unprecedented supramolecular architectures, that sets markedly apart from other innovative synthetic approaches related to CDS chemistry such as the subcomponent self-assembly approach.[18]

Our results reveal that the typical features of the coordination chemistry of Cu(I) ion (labile, flexible and low-directional coordination spheres) that were initially regarded as being strongly restrictive for the use of this ion in CDS chemistry turn out to be very valuable to conduct successfully the unprecedented reported syntheses. Due to a suitable molecular design of pre-assembled Cu(I) polymetallic building blocks, these limitations not only can be circumvented but also can be exploited to pave the way for innovative adaptative CDS processes. Obviously, another key factor in these reactions is the use of cyano-based precursors whose general labile coordination behavior[19] also promotes such concerted processes. Therefore, appropriate choice of the building blocks involved in adaptive CDS syntheses carries a great importance in order to probe, understand and extend the scope of this alternative synthetic approach.

Lastly but not the least, due to the versatile intrinsic photophysical properties of Cu(I) metal centers (including TADF behaviors), these new supramolecular syntheses prospects also allow one to draw great perspectives in the ready design of innovative inexpensive luminescent supramolecular compounds. Indeed, our results show that the photophysical performances of the luminescent Cu(I) building blocks embedded within intricate CDS assemblies can benefit from different valuable features: Cu(I) metal centers present in polycyclic supramolecular scaffolds having constrained geometries are associated with significantly reduced possibility of structural re-organization of their coordination sphere in the excited states. Therefore the non-radiative deactivation pathways that can be highly detrimental for the photophysical performances of Cu(I) coordination complexes are here greatly minimized. Moreover, the possibility of easily associating Cu(I) ions with heavy metal centers bearing high spin-orbit coupling constants allows more efficient radiative deactivation pathways, revealing an original 'heavy atom effect' to promote photoluminescence performances of Cu(I)-based luminophores. A general entry to new photoluminescent compounds having a large diversity of unconventional photophysical behaviors is therefore offered by this new adaptive CDS synthetic approach.

Conflicts of interest

There are no conflicts to declare.

Acknowledgements

This work was supported by the ANR (P-OPTOELECTR-MOLMAT), the French Research Ministry and the CNRS. C.L. thanks the Alexander von Humboldt Foundation for a fellowship for experienced researcher. Computations were performed using HPC resources from GENCI-CINES/IDRIS

(Grants A0040800649 and A0060800649). V.W.-W.Y. acknowledges support from The University of Hong Kong and the URC Strategically Oriented Research Theme on Functional Materials for Molecular Electronics. This work has been supported by the University Grants Committee Areas of Excellence (AoE) Scheme (AoE/P-03/08) and a General Research Fund (GRF) grant from the Research Grants Council of the Hong Kong Special Administrative Region, P. R. China (HKU 17334216).

Notes and references

1 (a) S. Pullen and G. H. Clever, *Acc. Chem. Res*., 2018, **51**, 3052–3064. (b) M. Käseborn, J. J. Holstein, G. H. Clever and A. Lützen, *Angewandte Chemie International Edition*, 2018, **57**, 12171–12175. (c) M. Piot, B. Abécassis, D. Brouri, C. Troufflard, A. Proust and G. Izzet, *PNAS*, 2018, **115**, 8895–8900. (d) V. Martínez-Agramunt, D. G. Gusev and E. Peris, *Chemistry – A European Journal*, 2018, **24**, 14802–14807. (e) V. Martínez-Agramunt, T. Eder, H. Darmandeh, G. Guisado-Barrios and E. Peris, *Angew. Chem. Int. Ed.*, 2019, **58**, 5682–5686. (f) A. Jana, S. Mandal, K. Singh, P. Das and N. Das, *Inorg. Chem*., 2019, **58**, 2042–2053. (g) S. Gaikwad, M. L. Saha, D. Samanta and M. Schmittel, *Chem. Commun.*, 2017, **53**, 8034–8037. (h) P. K. Biswas, S. Saha, Y. Nanaji, A. Rana and M. Schmittel, Inorg. Chem., 2017, **56**, 6662–6670. (i) Z.-Y. Li, J.-W. Dai, M. Damjanović, T. Shiga, J.-H. Wang, J. Zhao, H. Oshio, M. Yamashita and X.-H. Bu, *Angew. Chem. Int. Ed.*, 2019, **58**, 4339–4344. (j) M. Elsayed Moussa, S. Evariste, B. Krämer, R. Réau, M. Scheer and C. Lescop, *Angew. Chem. Int. Ed.,* 2018, **57**, 795–799. (k) M. Yamagami, T. Sawada and M. Fujita, *J. Am. Chem. Soc.* 2018, **140**, 8644-8647. (l) A. N. Oldacre, Al. E. Friedman and T. R. Cook, *J. Am. Chem. Soc.*, 2017, **139**, 1424–1427. (m) R. Zhu, I. Regeni, J. J. Holstein, B. Dittrich, M. Simon, S. Prévost, M. Gradzielski and G. H. Clever, *Angew. Chem. Int. Ed.* 2018, **57**, 13652-13656. (n) V. Vreshch, M. El Sayed Moussa, B. Nohra, M. Srebo, N. Vanthuyne, C. Roussel, J. Autschbach, J. Crassous, C. Lescop and R. Réau, *Angew. Chem. Int. Ed.,* 2013, **52**, 1968-1972. (o) Y. Yao, W. Shen, B. Nohra, C. Lescop, R. Réau, Chem. Eur. J., 2010, **16**, 7143-7163.

2 (a) T. R. Cook and P. J. Stang, *Chem. Rev.* 2015, **115**, 7001-7045. (b) K. Harris, D. Fujita and M. Fujita, *Chem. Comm.* 2013, **49,** 6703-6712. (c) M. Han, D. M. Engelhard and G. H. Clever, *Chem. Soc. Rev.* 2014, **43,** 1848−1860. (d) S. Zarra, D. M. Wood, D. A. Roberts and J. R. Nitschke, *Chem. Soc. Rev.* 2015, **44,** 419−432. (e) W. Wang, Y-. X. Wang and H.-B. Yang, *Chem. Soc. Rev.* 2016, **45**, 2656-2693. (f) C. Lescop, *Acc. Chem. Res.*, 2017, ***50***, 885-894. (g) S. Saha, I. Regeni, G. H. Clever, *Coord. Chem. Rev.* **2018,** ***374***, 1-14.

3 (a) M.L. Saha, X. Yan and P.J. Stang, *Acc. Chem. Res.* 2016, **49**, 2527−2539. (b) M. Zhang, M. L. Saha, M. Wang, Z. Zhou, B. Song, C. Lu, X. Yan, X. Li, F. Huang, S. Yin and P. J. Stang, *J. Am. Chem. Soc.* 2017, **139**, 5067−5074. (c) Y. Zhang, M. R. Crawley, C. E. Hauke, A. E. Friedman and T. R. Cook, *Inorg. Chem.* 2017, **56**, 4258−4262. (d) C.E Hauke, A. N. Oldacre, C.R.P. Fulong, A. E. Friedman and T. R. Cook, *Inorg. Chem.* 2018, **57**, 3587−3595. (e) Y. Hang, C. R. P. Fulong, C. E. Hauke, M. R. Crawley, A. E. Friedman and T. R. Cook, *Chem. Eur. J.* 2017, **23**, 4532-4536. (f) J. R. Shakirova, E. V. Grachova, V. Gurzhiy, V. Kumar S. Thangaraj, J. Jänis, A. S. Melnikov, A. J. Karttunen, S. P. Tunik and I. O. Koshevoy, *Angew. Chem. Int. Ed.* 2018, **57,** 14154-14158. (g) D. R. Martir and E. Zysman-Colman *Chem. Commun.* 2019, **55**, 139-158.

4 (a) J. E. M. Lewis, A. B. S. Elliott, C. J. McAdam, K. C. Gordon, J. D. Crowley, *Chem. Sci.* 2014, **5**, 1833–1843. (b) A. B. S. Elliott, J. E. M. Lewis, H. van der Salm, C. J. McAdam, J. D. Crowley and K. C. Gordon, *Inorg. Chem.* 2016, **55**, 3440−3447; (c) A. Schmidt, M. Hollering, J. Han, A. Casini and F. E. Kühn, *Dalton Trans.* 2016, **45**, 12297–12300. (d) X. Li, J. Wu, C. He, R. Zhang, C. Duan, *Chem. Commun.* 2016, **52**, 5104-5107. (e) D. Rota Martir, D. Escudero, D. Jacquemin, D. B. Cordes, A. M. Z. Slawin, H. A. Fruchtl, S. L. Warriner and E. Zysman-Colman, *Chem. Eur. J.* 2017, **23**, 14358–14366. (f) O. Chepelin, J. Ujma, X. Wu, A. M. Z. Slawin, M. B. Pitak, S. J. Coles, J. Michel, A. C. Jones, P. E. Barran and P. J. Lusby, *J. Am. Chem. Soc.* 2012, **134***,* 19334−19337. (g) V. E. Pritchard, D. Rota Martir, S. Oldknow, S. Kai, S. Hiraoka, N. J. Cookson, E. Zysman-Colman and M. J. Hardie, *Chem. Eur.J.* 2013, **23**, 6290–6294. (h) L. Schneider, V. Sivchik, K.-Y. Chung, Y.-T. Chen, A. J. Karttunen, P.-T. Chou and I. O. Koshevoy, *Inorg. Chem.* 2017, **56**, 4459−4467. (i) S. M. Woessner, J. B. Helms, Y. Shen and B. P. Sullivan, *Inorg. Chem.* 1998, **37,** 5406-5407. (j) R. J. Puddephatt, *Chem. Soc. Rev.* 2008, **37,** 2012-2027. (k) P. H. Dinolfo, M. E. Williams, C. L. Stern and J. T. Hupp, *J. Am. Chem. Soc*. 2004, **126**, 12989-13001. (l) J.-L. Zhu, Y.-Y. Ren, Y. Zhang, X. Liu, G.-Q. Yin, B. Sun, X. Cao, Z. Chen, X.-L. Zhao, H. Tan, J. Chen, X. Li and H.-B. Yang, *Nature Communications* 2019, **10**, DOI : 10.1038/s41467-019-12204.

5 (a) R. Czerwieniec, M. J. Leitl, H. H. H. Homeier and H. Yersin, *Coord. Chem. Rev.*, 2016, **325**, 2-28. (b) A. Kobayashi and M. Kato, *Chem. Lett.*, 2017, **46**, 154-162. (c) Q. Benito, X. Le Goff, S. Maron, A. Fargues, A. Garcia, C. Martineau, F. Taulelle, S. Kahlal, T. Gacoin, J.-P. Boilot and S. Perruchas, *J. Am. Chem. Soc.*, 2014, 136, 11311-11320. (d) B. Huitorel, H. El Moll, R. Utrera-Melero, M. Cordier, A. Fargues, A. Garcia, F. Massuyeau, C. Martineau-Corcos, F. Fayon, A. Rakhmatullin, S. Kahlal, J.-Y. Saillard, T. Gacoin and S. Perruchas, *Inorg. Chem.,* 2018*, **57,*** 4328-4339. (e) J. Nitsch, F. Lacemon, A. Lorbach, A. Eichhorn, F. Cisnetti and A. Steffen, *Chem. Commun.,* 2016, **52**, 2932-2935. (f) B. Hupp, J. Nitsch, T. Schmitt, R. Bertermann, K. Edkins, F. Hirsch, I. Fischer, M. Auth, A. Sperlich and A. Steffen, *Angew. Chem. Int. Ed.,* **2018**, ***57***, 13671-13675. (g) B. Hupp, C. Schiller, C. Lenczyk, M. Stanoppi, K. Edkins, A. Lorbach and A. Steffen, *Inorg. Chem.,* **2017**, ***56***, 8996-9008. (h) T. Hasegawa, A. Kobayashi, H. Ohara, M. Yoshida and M. Kato, *Inorg. Chem.*, 2017, **56**, 4928-4936. (i) C. Zheng, N. Wang, T. Peng and S. Wang, *Inorg. Chem.*, 2017, **56**, 1616-1625. (j) A. Kobayashi, M. Fujii, Y. Shigeta, M. Yoshida and M. Kato, *Inorg. Chem*., 2019, **58**, 4456–4464. (k) A. Kobayashi, Y. Yoshida, M. Yoshida and M. Kato, *Chem. Eur. J.*, 2018, **24**, 14750–14759. (l) P. Liang, A. Kobayashi, W. M. C. Sameera, M. Yoshida and M. Kato, *Inorg. Chem.*, 2018, **57**, 5929–5938. (m) A. V. Artem'ev, M. R. Ryzhikov, I. V. Taidakov, M. I. Rakhmanova, E. A. Varaksina, I. Y. Bagryanskaya, S. F. Malysheva and N. A. Belogorlova, *Dalton Trans.*, 2018, **47**, 2701–2710. (n) A. V. Artem'ev, E. A. Pritchina, M. I. Rakhmanova, N. P. Gritsan, I. Y. Bagryanskaya, S. F. Malysheva and N. A. Belogorlova, *Dalton Trans.*, 2019, **48**, 2328–2337. (o) G. Chakkaradhari, T. Eskelinen, C. Degbe, A. Belyaev, A.S. Melnikov, E.V. Grachova, S.P. Tunik, P. Hirva and I. O. Koshevoy, *Inorg. Chem.*, 2019, **58**, 3646-3660. (p) G. Chakkaradhari, Y.-T. Chen, A. J. Karttunen, M. T. Dau, J. Jänis, S. P. Tunik, P.-T. Chou, M.-L. Ho and I. O. Koshevoy, *Inorg. Chem.*, 2019, **58**, 2174-2184. (q) R. Hamze, J. L. Peltier, D. Sylvinson, M. Jung, J. Cardenas, R. Haiges, M. Soleilhavoup, R. Jazzar, P. I. Djurovich, G. Bertrand and M. E. Thompson, *Science.,* **2019**, **363**, 601-606. (r) S. Shi, M. Chul Jung, C. Coburn, A. Tadle, M. R. D. Sylvinson, P. I. Djurovich, S. R. Forrest and M. E. Thompson, *J. Am. Chem. Soc.*, **2019**, **141**, 3576-3588.

6 H. Yersin, Highly Efficient OLEDS: Materials Based on Thermally Activated Delayed Fluorescence, 2019, Wiley-VCH Verlag GmbH & Co.

7 (a) M. El Sayed Moussa, S. Evariste, H.-L. Wong, L. Le Bras, C. Roiland, L. Le Polles, B. Le Guennic, K. Costuas, V. W.-W. Yam and C. Lescop, *Chem. Comm*., 2016, **52**, 11370-11373; (b) S. Evariste, A.M. Khalil, M. El Sayed Moussa, A. K.-W. Chan, E. Y.-H. Hong, H.-L. Wong, B. Le Guennic, G. Calvez, K. Costuas, V. W.-W. Yam and C. Lescop, *J. Am. Chem. Soc.,* 2018, **140**, 12521–12526.

8 For experimental details, yield calculations, spectroscopic, X-ray diffraction data and computational studies, see SI.

9 Equal relative occupancies for C and N atoms have been modelled at the atomic position determined for the cyano ligands connecting two Cu(I) metal centers. For the $M(CN)_x$ fragments (M = Au, Pt), C atoms have been assigned to the atoms connected to the M(II) metal centres, see: L. Schneider, V. Sivchik, K.-Y. Chung, Y.-T. Chen, A. J. Karttunen, P.-T. Chou and I. O. Koshevoy, *Inorg. Chem.,* 2017, **56**, 4459-4467.

10 Comparing the solid-state structures of **A** and **1**, no major differences regarding stabilizing intermolecular interaction are observed in the crystal packing that could induce a selection during crystallization process.

11 A. Belyaev, T. Eskelinen, T. Minh Dau, Y. Y. Ershova, S. P. Tunik, A. S. Melnikov, P. Hirva and I. O. Koshevoy, *Chem. Eur. J.*, 2018, **6**, 1404-1415.

12 H. Schmidbaur and A. Schier, *Chem. Soc. Rev,* 2012, **41**, 370-412.

13 V. Vreshch, W. Shen, B. Nohra, S.-K. Yip, V.W.-W. Yam, C. Lescop and R. Réau, *Chem. Eur. J.*, 2012, **2**, 466-477.

14 (a) G. Glieman and H. Yersin, *Struct. Bonding*, 1985, **62**, 87-153; (b) V. W.-W. Yam, V. K.-M. Au and S. Y.-L. Leung, *Chem. Rev.* 2015, **115**, 7589-7728; (c) K. M.-C. Wong, M.-Y. Chan and V. W.-W. Yam, *Adv. Mater.,* 2014, **26**, 5558-5568; (d) K. M.-C. Tang, A. K.-W. Chan, M.-Y. Chan and V. W.-W. Yam, *Top Curr Chem*, 2016, **374**, 1-43; (e) M. Yoshida and M. Kato, *Coord. Chem. Rev.,* 2018, **355**, 101–115; (f) C. A. Strassert, C.-H. Chien, M. D. Galvez Lopez, D. Kourkoulos, D. Hertel, K. Meerholz and L. De Cola, *Angew. Chem. Int. Ed.,* 2011, **123**, 976-980; (g) Y. Li, L. Chen, Y. Ai, E. Y.-H. Hong, A. K.-W. Chan and V. W.-W. Yam, *J. Am. Chem. Soc.*, 2017, 139, 13858–13866.

15 M. M. Wu, L. Y. Zhang, Y. H. Qin and Z. N. Chen, *Acta Cryst.,* 2003, **E59**, m195-m196.

16 Signal typical of free dppm ligand in solution were never observed in the $^{31}P\{^{1}H\}$ NMR spectra recorded during these reactions.

17 Along the series of derivatives **A**, $\mathbf{C_{pt}}$ and **3**, the tetrametallic assembly **A** present the lowest solubility in chlorinated solvents. This allows precluding the possibility of a selection in the reported syntheses that would be due to the crystallization of the less soluble species.

18 (a) D. Zhang, T.K. Ronson and J. R. Nitschke, *Acc. Chem. Res.,* 2018, **51**, 2423-2436; (b) S. M. Jansze and K. Severin, *Acc. Chem. Res.,* 2018**, 51**, 2139-2147.

19 L. M. C. Beltran and J. R. Long, *Acc. Chem. Res.,* 2005, **38**, 325-334.